Journal of Alloys and Compounds 527 (2012) 96–100

Contents lists available at SciVerse ScienceDirect

Journal of Alloys and Compounds

journal homepage: www.elsevier.com/locate/jallcom

The effect of nickel nanostructure on surface waves propagation in silicon support

A. Trzaskowska[a,*], S. Mielcarek[a], B. Graczykowski[a], B. Mroz[a], P. Patoka[b], M. Giersig[b]

[a] Faculty of Physics, Adam Mickiewicz University, Umultowska 85, 61-614 Poznan, Poland
[b] Institut für Experimentalphysik, Freie Universität Berlin, 14195 Berlin, Germany

ARTICLE INFO

Article history:
Received 31 January 2012
Received in revised form 29 February 2012
Accepted 2 March 2012
Available online xxx

PACS:
63.22.−m
43.35.Pt
78.35.+c

Keywords:
Nanostructures
Surface phonons
Brillouin spectroscopy

ABSTRACT

Surface Brillouin spectroscopy was applied to characterise the dynamics of surface acoustic waves in a silicon-based nanocomposite. The propagation velocities of Rayleigh phonons and their anisotropy in silicon support (1 1 1) loaded with a nanosized nickel island structure were determined. Deposition of a 2D nickel nanostructure on silicon substrate leads to the appearance of new peaks in the Brillouin spectrum.

1. Introduction

Elastic properties of nanostructural materials are of profound importance from the viewpoint of their application in microelectronics, photonics or in nano-electro-mechanical systems. Recently of great interest are the elastic properties of a silicon support loaded with nanostructures of different types [1–3]. 2D periodic nanostructure made of materials of different elastic properties have been an attractive subject of research over the past decade. Such structures may have properties typical to the phononic crystals [4–9]. A nanostructure can be introduced as point-pattern or as a uniform layer [10,11]. Evaluation of elastic properties of such systems is possible on the basis of behaviour of surface acoustic waves (SAW) propagating in the support by the surface Brillouin light scattering (BLS) [12,13]. This method is non-invasive and permits investigation of nanometric size systems with no risk of their damage [14,15]. Taking into regard the nature of surface acoustic waves, i.e. their disappearance with increasing depth, deposition of a load on the support can significantly change the surface elastic properties of the silicon support.

The nanostructures were produced by the nanosphere lithography [16–18]. By placing masks made of polystyrene (PS)-latex beads on the support on which loading materials are evaporated it is possible to obtain honeycomb lattices of triangularly shaped islands of those materials on various substrates. In this study the substrate was silicon (1 1 1) whilst the loading material was nickel. Our previous work reported on the elastic properties of silicon surfaces covered with low nickel islands [19]. In this study the height of the nickel islands was changed but their mutual distances were kept the same.

The aim of this study was to establish the effect of a periodic nickel nanostructure of different heights on the silicon substrate. On the basis of behaviour of Rayleigh-type surface acoustic waves (SAW), the phase velocity and anisotropy of phonons propagating in the (1 1 1) plane of silicon substrate were determined for different heights of the nickel island structure deposited on the silicon surface.

2. Experimental procedure

2.1. The samples

The samples used in experiments were made by our partner at the Freie Universität Berlin by the use of the well-established method of nanosphere lithography [20–22]. The samples were in the size of 1 cm × 1 cm. The process of production of such nanostructures is realised in three stages: deposition of monolayer PS-latex beads onto the silicon support, deposition of nickel by electron beam evaporation system and washing off (dissolution) the PS-latex mask. The diameter of the bead used was 540 nm. As a result of this process the silicon support samples with deposited nickel nanostructure of pseudo-hexagonal symmetry are obtained. Depending on the evaporation time, maintaining a constant deposition rate, the resulting nanostructures have different heights. The topography of the samples was determined by atomic force microscopy (Nanosurf AFM – Easy Scan) at room

* Corresponding author.
E-mail address: olatrzas@amu.edu.pl (A. Trzaskowska).

0925-8388/$ – see front matter © 2012 Elsevier B.V. All rights reserved.
doi:10.1016/j.jallcom.2012.03.011

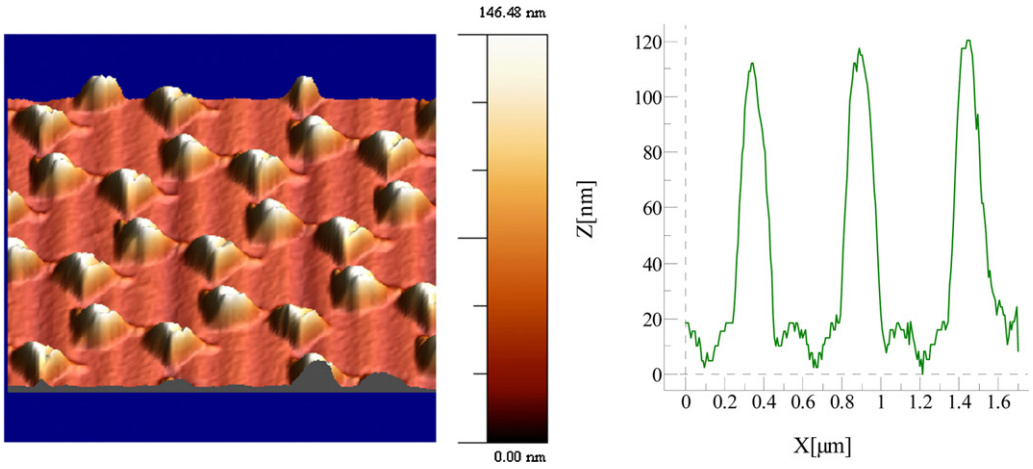

Fig. 1. AFM images of nickel particles deposited through 540 nm PS-latex bead masks making nanostructures of height 100 nm.

temperature in the contact mode. The size of the mapped area was about 2 μm × 2 μm. Image of exemplary surface topography of the studied structures is shown in Fig. 1.

Nickel islands on the silicon surface in the macro scale show a clear pseudo-hexagonal symmetry. The symmetry of the nano-island structure deposited is rotated by 6° with respect to the crystallographic axes of the silicon support. The cross-sections of topographic images of the sample surfaces permitted determination of the heights of the five nickel nanostructures as 25, 50, 100, 120 and 140 nm. Assuming the ideal conditions of nickel islands deposition, the coverage of the silicon surface was estimated as minimum 9%. This result is obtained on neglecting the effect of the islands smear at the bases. As follows from mathematical considerations, the silicon surface coverage does not depend on the diameters of the latex beads used, however, according to AFM topographic analysis, the real coverage was slightly greater because of the smear of the nickel islands, which was shown in Fig. 1. The stress induced by the island nanostructure modifies the propagation of surface waves in the silicon substrate. The magnitude of the stress is related to the height of the nickel islands and thus to the loading of the silicon surface.

2.2. Experimental setup

Elastic properties of the silicon surfaces covered with nickel nanostructure were studied with the use of tandem type Brillouin interferometer (JRS Scientific Instruments) ensuring the contrast of 10^{10} [23]. The source of light used was an Nd:YAG single-mode diode-pumped laser of power 200 mW, emitting the second harmonics of the length $\lambda_0 = 532$ nm (Excelsior Spectra Physics). Detailed description of the experimental setup can be found in [24,25]. The light incident on the sample was polarised in the sagittal plane defined by the wave vector of a given phonon and normal to the sample surface. Measurements were made in the backscattering geometry (180°). The backscattered light was collected by using f/8 optics, focal length 58 mm. The solid angle α of the lens was 0.63 ss. Measurements were performed for the free spectral range of 20 GHz. The surface phonon wavenumber k_R is:

$$k_R = \frac{4\pi}{\lambda_0}\sin\Theta \tag{1}$$

where Θ is the angle of light incidence to the normal to the sample surface. The Θ angle was varied in the range 14–70°. The wavenumber of the phonons k_R varied from 0.57×10^7 m^{-1} to 2.21×10^7 m^{-1}. Brillouin spectroscopy permits investigation of elastic properties of the bulk as well as surface systems on the basis of phonon propagation velocity measurement. The velocity of surface phonons υ_R depends on $2\sin\Theta$ as follows from:

$$\Delta f_R = \frac{2\upsilon_R \sin\Theta}{\lambda_0} \tag{2}$$

where Δf_R is the surface Brillouin frequency shift [26,27].

For opaque crystalline samples, a linear dependence of the frequency of the mode on $2\sin\Theta$ is one of the criteria distinguishing the Rayleigh surface waves (RSW) in Brillouin spectra in backscattering geometry. No such relation is observed for bulk phonon frequency in this geometry. Another criterion needed to be satisfied to determine the character of modes propagating in a given material is that the velocity of surface modes (except so-called pseudo-surface waves) in a given material υ_R should be always lower than that of slowest transverse bulk modes υ_T:

$$\upsilon_R < \upsilon_T \tag{3}$$

The range of wavelengths of the Rayleigh surface phonons studied was from about 280 nm to 780 nm.

The study was performed for samples mounted on a special holder equipped with an angular nonius permitting position measurements to the accuracy of 0.1°. The holder permitted changes in the sample position in the horizontal plane and rotations of the sample around the normal to the sample surface (Fig. 2).

3. Velocity and anisotropy of surface phonons

Brillouin frequency shift of surface phonons was measured for the samples loaded with nickel nanostructures of different height deposited on the silicon surface (1 1 1). Analysis of Brillouin spectra recorded for different angles of light incidence for particular samples permitted determination of phase velocity of the Rayleigh-type SAW surface phonons according to Eq. (2), see Fig. 3. The velocity was determined for two propagation directions: $[\bar{1}\,1\,0]$ and $[1\,1\,\bar{2}]$. As follows from the angular dependencies of SAW phase velocity in the (1 1 1) plane, it goes through a minimum and maximum for these two directions, respectively. The measuring error in the SAW phase velocity at the precise angular arrangement is less than 12 m/s.

With increasing height of the nanostructure deposited on the silicon support, the velocity of propagation of Rayleigh surface phonon in both directions studied decreased. The maximum change in the phase velocity of SAW propagation reaching almost 8% was observed for silicon loaded with the nickel island nanostructure higher than 100 nm. Moreover, with increasing height of the nickel islands the difference in the velocity of phonons propagating in the directions $[\bar{1}\,1\,0]$ and $[1\,1\,\bar{2}]$, increases.

The anisotropy of surface phonon frequency was measured in the samples loaded with nickel nanostructures of different heights

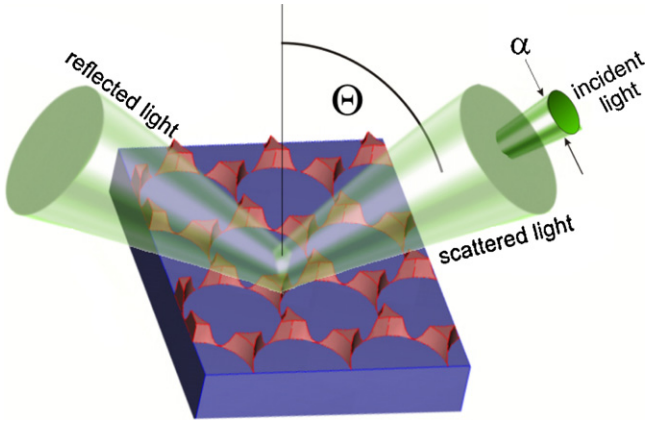

Fig. 2. Schematic presentation of the sample taking into account the geometry of the measuring BLS.

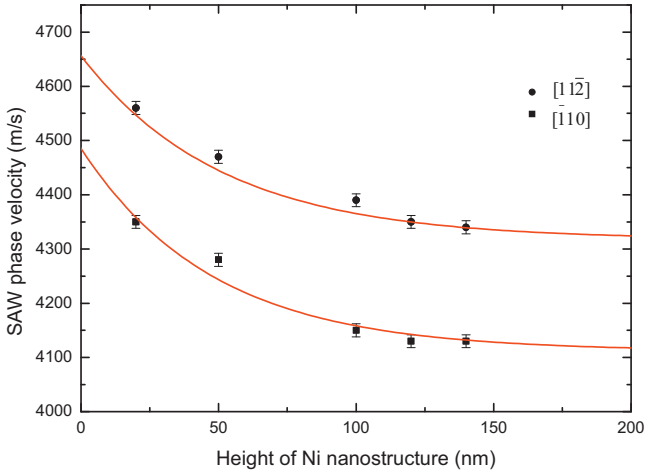

Fig. 3. Phase velocity of propagation of SAW phonons in silicon support versus the height of the nickel nanostructure. The solid line is the exponential fit to the measuring points.

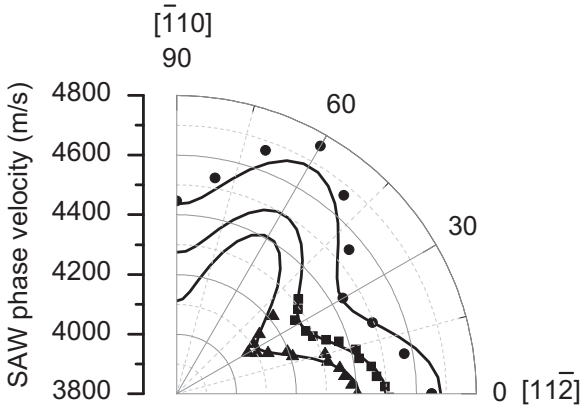

Fig. 4. Anisotropy of the velocity of SAW propagating in silicon (●), in silicon loaded with a nickel nanostructure of the height 50 nm (■) and 100 nm (▲), $\Theta = 30^{\circ}$. The solid line is the sinus function fit to the experimental points.

of the islands. Because of the cubic structure of the silicon support, the (1 1 1) plane has trigonal symmetry; thus, the anisotropy of SAW propagating in the (1 1 1) plane has a six-fold pattern (Fig. 4). On the macro-scale, the symmetry of the island nanostructure is

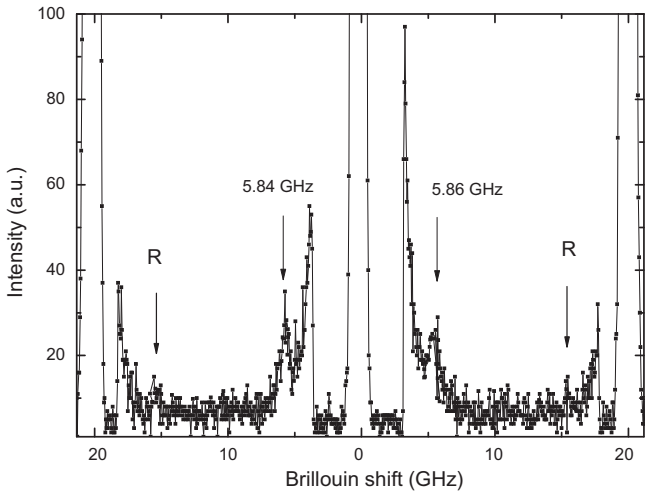

Fig. 5. An exemplary BLS spectrum of the Si surface loaded with a Ni nanostructure ($h = 100$ nm) with an additional phonon, $\Theta = 65^{\circ}$.

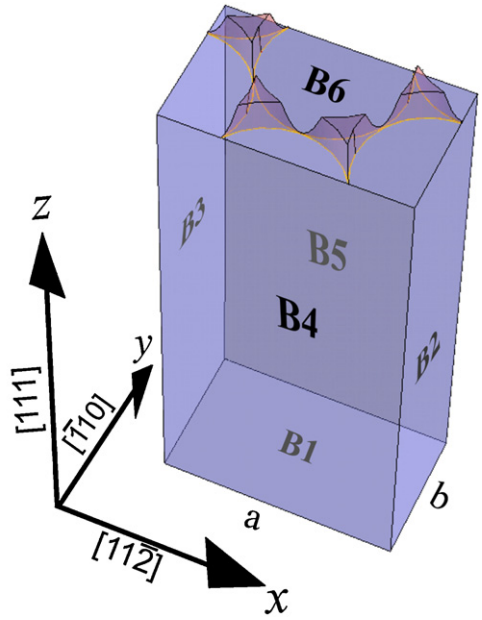

Fig. 6. Schematic presentation of the elementary cell used for the simulations by the FEM method.

pseudo-hexagonal, see Fig. 1. The Brillouin shift dependence on $2 \sin \Theta$ was measured for each sample for a few azimuthal angles in order to determine the Rayleigh-type SAW velocity. The dependence for a given angle is strictly linear, υ_R = constant for a defined azimuthal (in-plane) angle for the sample of pure silicon and silicon loaded with the nanoisland structure. For a given azimuthal angle each sample is characterised by a different velocity of the surface wave (Fig. 4). After deposition of the island nanostructure on the silicon surface, the character of anisotropy of the surface phonon propagating on the silicon surface is retained.

4. Additional phonon detected for high nanostructure

The loading with a nanostructure of islands ≥100 nm is a significant disturbance to the silicon surface and can change the elastic properties of the surface studied. Such a change was detected in the

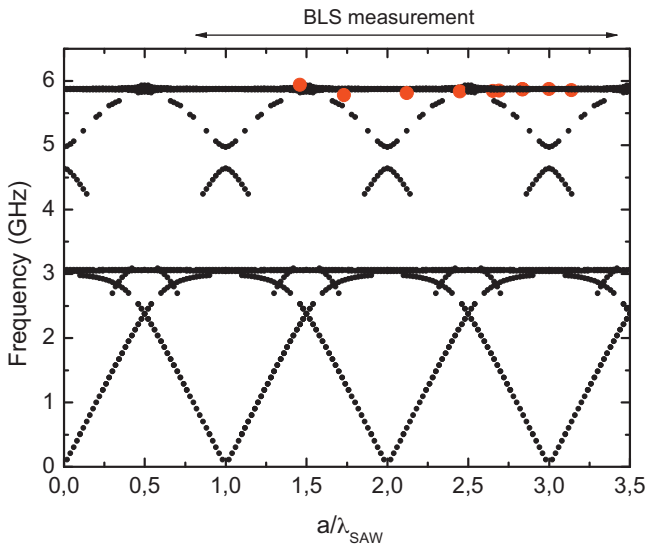

Fig. 7. The dispersion relation for SAW. Results of FEM simulations compared to the measured points (●) for a nanostructure of 100 nm.

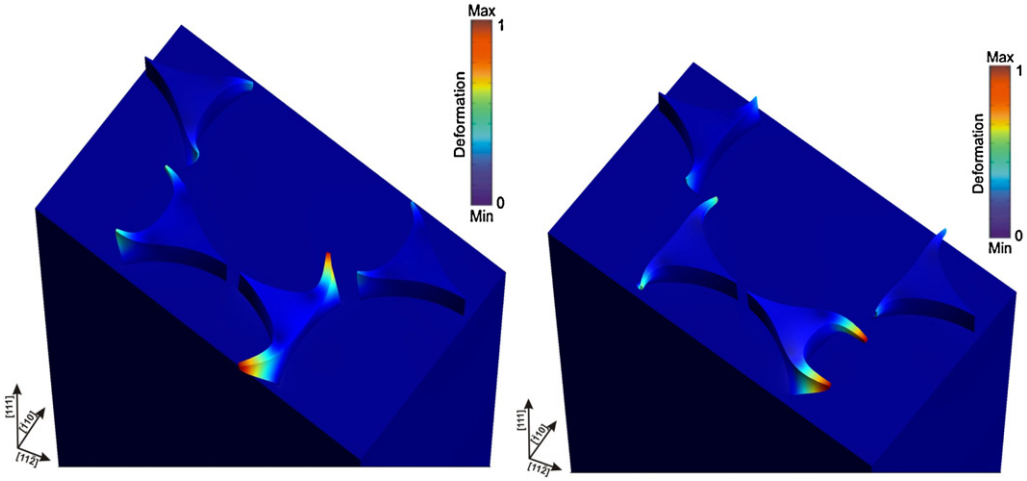

Fig. 8. The maps of deformations of the elementary cell appearing for the phonons in the BLS spectra for $\Delta f_{SAW} = 5.92$ GHz.

samples studied. The Brillouin spectra of the samples loaded with high nickel nanostructures revealed the presence of an additional phonon of a relatively low frequency (Fig. 5). The appearance of this additional phonon was accompanied by a decrease in the intensities of the peaks related to the Rayleigh-type SAW (R) present in the Brillouin spectra, e.g. Fig. 5.

The dispersion relation of the additional phonon appearing in the BLS spectra was established on the basis of measurements for a few Θ angles. Theoretical prediction of the dispersion relation for the nanostructure loaded samples needs advanced numerical simulation methods; we have applied the finite element method (FEM).

5. FEM simulation

To establish theoretically the dispersion relation for SAW propagating in the systems with nanostructures studied, the finite elements method (FEM) of simulations was applied. Schematic presentation of the elementary cell used in the simulations is shown in Fig. 6.

The silicon substrate was approximated by a cubic uniform elastic half-space $z \leq 0$ onto which a nanostructure of nickel islands of a specific height was loaded. The model assumes perfectly bonded, ideally flat material with zero interfacial thickness and uniform respective layer thickness, no roughness and defects, with constant elastic properties within a given layer. For the walls B2, B3, B4 and B5, the periodic Bloch–Floquet boundary conditions were expressed for each of the three (u,v,w) components of deformation. In order to get an exponential decay of the wave amplitude with depth, free boundary conditions were assumed for B6 and all nanostructure's walls and fixed boundary conditions for B1 wall.

The calculations were performed for the elastic constants of cubic silicon $C_{11} = 165.7$ GPa, $C_{12} = 63.9$ GPa, $C_{44} = 79.9$ GPa and density $\rho_{Si} = 2331\ \mathrm{kg\,m^{-3}}$ [28], and isotropic nickel, $C_{11} = 311.5$ GPa, $C_{12} = 125.7$ GPa, and density $\rho_{Ni} = 8908\ \mathrm{kg\,m^{-3}}$ [29]. Taking into account the orientation of the silicon substrate in the (1 1 1) plane, the fundamental components of the elasticity tensor were rotated accordingly. To calculate the dispersion diagrams of phononic band structures, the COMSOL MULTIPHYSICS software was used [30]. By imposing certain filters on FEM simulation results it is possible to exclude certain specific waves e.g. no results related to bulk wave propagation are obtained. Analysis of the results with different filters imposed has shown that the energy of deformation must be concentrated near the surface and the total deformation is as much as possible parallel to the wave vector.

The dispersion relations obtained for the phonons propagating in the $[1\,1\,\bar{2}]$ direction are shown in Fig. 7.

The measured points were obtained on the basis of BLS data for a few angles of light incidence. Interestingly, the frequency of the additional phonon does not depend on the wavenumber. Analysis of the activity of this new phonon versus the light beam polarisation has shown that this phonon is visible only when the incident light is polarised in the sagittal plane and the scattered beam is non-polarised. For the phonon of 5.92 GHz the mechanical energy is concentrated in the nickel islands. The corresponding vibrations of the islands are called the eigen vibrations and are transferred through the silicon substrate which is only slightly deformed. Graphical presentation of the field of deformations characteristic of the phonon of 5.92 GHz visible in the BLS spectra, is given in Fig. 8.

In order to illustrate the island deformation fields the images in Fig. 8 are shifted in time. The maps of deformation shown in Fig. 8 evidence that the mode of 5.92 GHz visible in the BLS spectra corresponds to differing in phase displacement of the islands. The total deformation is consistent with the direction of wave propagation. The differences in the nickel islands deformations follow from the fact that the mechanical energy is transferred through the silicon substrate from one island to another.

6. Conclusions

Brillouin spectroscopy study permitted characterisation of surface elastic properties of silicon loaded with nickel island nanostructures. With increasing height of the nickel nanostructure, the SAW propagation velocity in the silicon substrate decreases.

The anisotropy of the Rayleigh surface phonons propagating in silicon substrate proved that with increasing height of the nanostructure the difference in frequencies of the phonons propagating in the directions $[\bar{1}\,1\,0]$ and $[1\,1\,\bar{2}]$ increases. After deposition of a nickel nanostructure on silicon substrate, the hexagonal pattern of anisotropy of the surface Rayleigh wave propagation velocity is enhanced with growing height of the nanoislands.

Simulation of the dispersion relations in the samples studied permitted classification of the additional phonon detected in the BLS spectra. This mode appears as a result of vibrations of the nickel islands transferred through the silicon substrate which is only slightly deformed. So we can conclude that mechanical energy is localised in the islands.

Periodicity of the island nanostructure and type of materials used (silicon and nickel) suggest a possibility of phononic and

magnonic properties in the systems studied. Investigation aimed at determination of these properties and in particular at proving the existence of an energy gap is underway.

Acknowledgements

This work has been partially supported by Grant No. N202 230637 from the Polish Ministry of Science and Higher Education. MG thanks for the financial support by the Nanoscale Project FU Berlin.

References

[1] Y. Li, H.S. Lim, S.C. Ng, M.H. Kuok, M.Y. Ge, J.Z. Jiang, Appl. Phys. Lett. 91 (2007) 093116-1–093116-3.
[2] P.R. Heyliger, C.M. Flannery, W.L. Johnson, Nanotechnology 19 (2008) 145707-1–145707-9.
[3] J.W. Jonson, S.A. Kim, R. Geiss, C.M.L. Soles, C. Wang, C.M. Stafford, W.-L. Wu, J.M. Torres, B.D. Vogt, P.R. Heyliger, Nanotechnology 21 (2010) 075703-1–075703-8.
[4] Y. Pennec, B. Djafiri-Rouhani, H. Larabi, J.O. Vasseur, A.C. Hladky-Hennion, Phys. Rev. B 78 (2008) 104105-1–104105-8.
[5] Y. Penneca, J.O. Vasseur, B. Djafari-Rouhani, L. Dobrzyński, P.A. Deymierb, Surf. Sci. Rep. 65 (2010) 229–291.
[6] M. Oudich, M.B. Assouar, Appl. Phys. Lett. 99 (2011) 123505-1–123505-3.
[7] N. Gomopoulos, D. Maschke, C.Y. Koh, E.L. Thomas, W. Tremel, H.-J Butt, G. Fytas, Nano Lett. 10 (2010) 980–984.
[8] T. Still, W. Cheng, M. Retsch, R. Sainidou, J. Wang, U. Jonas, N. Stefanou, G. Fytas, Phys. Rev. Lett. 100 (2008) 194301-1–194301-4.
[9] W. Cheng, J. Wang, U. Jonas, G. Fytas, N. Stefanou, Nat. Mater. 5 (2006) 830–836.
[10] K. Van Workum, J.J. de Pablo, Nano Lett. 3 (2003) 1405–1410.
[11] A.G. Every, B.A. Mathe, J.D. Comins, Ultrasonics 44 (2006) e929–e934.
[12] T. Witkowski, G. Distler, K. Jung, B. Hillebrands, J.D. Comins, Phys. Rev. B 69 (2004) 205401–205409.
[13] X. Zhang, J.D. Comins, A.G. Every, P.R. Stoddart, W. Pang, Phys. Rev. B 58 (1998) 13677–13685.
[14] T. Gorishnyy, C.K. Ullal, M. Maldovan, G. Fytas, E.L. Thomas, Phys. Rev. Lett. 94 (2005) 115501–115504.
[15] S.O. Demokritov, V.E. Demidov, IEEE Trans. Magn. 44 (2008) 6–12.
[16] Z.P. Huang, D.L. Carnahan, J. Rybczynski, M. Giersig, M. Sennett, D.Z. Wang, J.G. Wen, K. Kempa, Z.F. Rena, Appl. Phys. Lett. 82 (2003) 460–462.
[17] K. Kempa, B. Kimball, J. Rybczynski, Z.P. Huang, P.F. Wu, D. Steeves, M. Sennett, M. Giersig, D.V.G.L.N. Rao, D.L. Carnahan, D.Z. Wang, J.Y. Lao, W.Z. Li, Z.F. Ren, Nano Lett. 3 (2003) 13–18.
[18] Y. Zhang, X. Wang, Y. Wang, H. Liu, J. Yang, J. Alloys Compd. 452 (2008) 473–477.
[19] A. Trzaskowska, S. Mielcarek, B. Mroz, M. Giersig, W. Kandulski, Surf. Sci. 601 (2007) 2330–2338.
[20] J. Rybczyński, PhD Thesis, Poznań University of Technology, 2003.
[21] J. Rybczynski, U. Ebels, M. Giersig, Colloids Surf. A 219 (2003) 1–6.
[22] A. Kosiorek, W. Kandulski, P. Chudzinski, K. Kempa, M. Giersig, Nano Lett. 4 (2004) 1359–1363.
[23] J.R. Sandercock, in: M. Cardona, G. Güntherodt (Eds.), Light Scattering in Solids, Topics in Applied Physics, vol. 51, Springer, New York, 1982, pp. 173–206.
[24] A. Trzaskowska, S. Mielcarek, B. Graczykowski, F. Stobiecki, J. Alloys Compd. 517 (2012) 132–138.
[25] B. Mroz, S. Mielcarek, J. Phys. D: Appl. Phys. 34 (2001) 395–399.
[26] H.Z. Cummins, in: H.Z. Cummins, A.P. Levanyuk (Eds.), Light Scattering Near Phase Transitions, North-Holland, Amsterdam, 1983, pp. 359–447.
[27] R. Vacher, L. Boyer, Phys. Rev. B 6 (1972) 639–673.
[28] G.W. Farnell, in: W.P. Mason, R.N. Thurston (Eds.), Physical Acoustics, vol. 6, Academic Press, New York, 1970, pp. 109–166.
[29] G.W. Farnell, E.L. Adler, in: W.P. Mason, R.N. Thurston (Eds.), Physical Acoustics, vol. 6, Academic Press, New York, 1972, pp. 35–127.
[30] COMSOL, Multiphysics finite element software, COMSOL, AB, Sweden (2011).